Azerbaijani Astronomical Journal AAJ **21(1)**, 50–58 (2026) Accepted 31 May 2026 https://doi.org/10.59849/2078-4163.2026.1.50

THERMAL STRESSES IN SMALL BODIES APPROACHING THE SUN

R. Spassyuk[1]*, L. I. Shestakova[1]

[1] *V.G. Fesenkov Astrophysical Institute, Observatory 23, 050020 Almaty, Kazakhstan*

Last updated 2026 October 19; in original form 2026 November 28

ABSTRACT

This study examines thermal stresses as one of the key physical mechanisms leading to the destruction of small Solar System bodies as they approach the Sun. The thermal destruction mechanism and its evolution are investigated in bodies of icy and silicate compositions of various sizes, along with their role in initiating cracking, fragmentation, and subsequent mass loss. Analytical and numerical solutions of the heat conduction equation for spherical bodies moving in highly eccentric orbits are used to describe temperature fields and resulting stresses. The analytical approach is based on the assumption of constant thermal diffusivity, whereas the numerical model accounts for its temperature dependence and the actual thermophysical properties of crystalline ice and meteoritic matter. A systematic comparison of the two methods was conducted for bodies ranging in size from decimeter-sized meteoroids to kilometer-sized cometary nuclei. It is shown that thermal stresses can exceed the material strength limits at significant heliocentric distances that is, well before reaching the tidal disruption zone. It is also shown that the analytical method performs effectively and exhibits minor discrepancies when compared with the numerical method. It was found that intermediate-sized bodies are the most vulnerable, as strong temperature gradients form between the cold core and heated surface layers. Small bodies heat up almost entirely and do not accumulate significant internal stresses, while large objects maintain stability due to the low penetration of heat into the interior. The results obtained confirm the significant role of thermal stresses in the evolution, activity, and destruction of both cometary nuclei and small asteroid bodies.

Key words: Small bodies – Comets – Asteroids – Thermal stresses – Numerical calculations

1 INTRODUCTION

This chapter provides a general overview of the key aspects related to the disintegration of small Solar System (SS) bodies.

Despite the large number of observed comets, the mechanisms of their formation, evolution, and disintegration remain not fully understood. Agglomeration models suggest that comets are loose bodies with high porosity (up to ∼80%) and low density of approximately 0.2 g/cm^3 making them vulnerable to destruction by tidal forces Sekanina et al. (1994). At the same time, a number of studies point to higher density values, reaching 0.5-0.6 g/cm^3 Solem (1995).

Significant discrepancies also exist in estimates of the initial sizes of cometary nuclei. A survey of long-period comets shows that disintegrating nuclei have substantially smaller sizes (average radius ∼0.4 km) compared to surviving ones (∼1.6 km), as well as smaller perihelion distances Jewitt (2022). This indicates an increased probability of the destruction of small nuclei during their approach to the Sun. In a number of works, the destruction of comets near the Sun is attributed to breakup caused by the rotation of the nucleus Sekanina (1997). Additionally, other possible mechanisms of comet disintegration are discussed, including disruption by centrifugal forces, destruction due to internal gas pressure during intense sublimation, and collisions with other small bodies Boehnhardt (2005). Collectively, these processes are considered the primary causes of comet decay in the Solar System.

Regarding small bodies composed of silicate rocks, the origin regions of most meteorites and kilometer-sized near-Earth objects (NEOs), including some minor classes, have been identified to date Brož et al. (2024). The authors of that work examined 38 individual asteroid families, both young and old, and determined their contribution to the populations of near-Earth objects ranging in size from meters to kilometers using collision and orbital models. In work Brož et al. (2024), three young asteroid families (Karin, Koronis,

* E-mail: spassyuk@fai.kz

Massalia) were identified as the source of the majority of ordinary chondrite falls. The origin regions of various classes of meteorites and near-Earth objects have been determined, with an emphasis on various classes of carbonaceous chondrites. Some well-known annual meteor showers are formed as a result of the destruction of comets or active asteroids such as 3200 Phaethon, which is the parent body of the Geminid meteor shower Jewitt (2010).

In this work, we propose a mechanism for the destruction of small bodies made of crystalline ice and silicates due to thermal stresses. As cometary bodies approach the Sun, surface layers heat up, and heat is transferred inward. In bodies of homogeneous composition, this process can generate strong stresses exceeding the strength limits of the materials. This process was examined in Shestakova & Serebryanskiy (2023) for homogeneous bodies of water ice and with the inclusion of silicate inhomogeneities composed of ice and silicates. An analytical solution of the linear heat conduction equation for spherical bodies approaching the Sun along parabolic orbits was obtained in Shestakova & Tambovtseva (1997). Thermal stress has emerged as a probable fragmentation mechanism capable of operating far from the Sun without requiring tidal forces; studies show that thermal stresses can exceed the tensile strength of terrestrial materials. For small bodies of cometary and asteroidal origin, this mechanism operates at various heliocentric distances, which is due to significantly different thermal and physico-mechanical properties. This mechanism is responsible for the formation of near-surface cracks followed by material release and even complete fragmentation. What might happen next? A cracked object may enter the Roche limit and undergo complete disintegration, as was the case with comet SL9 Shestakova et al. (2025), or in the case of dust clouds, enter the sublimation zone. In such instances, thermal stresses determine the initial gradual splitting of the body. The subsequent evaporation of small bodies under the influence of solar heat allows for the acquisition of information regarding their chemical composition through infrared (IR) observations. Despite the unfavorable conditions for the existence of crystalline ice in space, recent spectroscopic studies of planetary satellites and Kuiper Belt objects have revealed signs of its presence. According to Prialnik & Jewitt (2022), modeling has demonstrated the possible crystallization of matter deep within the body under various orbital parameters. The spectral band of crystalline ice at 1.65 μm was detected in the satellites of Jupiter (Europa), Uranus Grundy et al. (2006); Guilbert et al. (2009); de Bergh et al. (2009), and Charon the satellite of Pluto Brown & Calvin (2000). Analysis of the spectrum of Phaethon in the mid-infrared region, obtained from the Spitzer Space Telescope, showed that Phaethon is associated with rare carbonaceous chondrites containing olivine, Mg-rich carbonates, and Fe-sulfides MacLennan & Granvik (2023, 2024). These minerals decompose at temperatures of approximately 1000 K, which 3200 Phaethon reaches at perihelion. The role of thermal stresses in the physics of small Solar System bodies has been studied by many authors Shestakova & Tambovtseva (1997); Tambovtseva & Shestakova (1999); Täuber & Kührt (1987); Čapek & Vokrouhlický (2010). We apply both analytical methods Shestakova & Tambovtseva (1997) and a new method for the numerical solution of the heat diffusion equation with one initial and two boundary conditions. The analytical approach assumes constant thermal diffusivity, whereas the numerical model accounts for temperature-dependent thermal diffusivity. The remaining structure of the article is as follows: the second section will consider the thermal and elastic properties of crystalline ice and silicate rocks. In the third section, a numerical model for the destruction of small bodies will be proposed; the fourth section will present the results of comparing the analytical and numerical models along with a statistical analysis and the conclusion.

2 THERMAL AND ELASTIC PROPERTIES OF CRYSTALLINE ICE AND SILICATE MATERIALS FRAGMENTS OF SMALL BODIES

Icy and silicate materials possess a diverse range of properties. Overall, they can be characterized by thermophysical (c_v, k, a^2) and physico-mechanical (E, μ) parameters as they vary with temperature. Here, c_v denotes the heat capacity at constant volume, and k represents thermal conductivity. E is the Young's modulus of elasticity (MPa), α is the coefficient of linear thermal expansion (expressed in K^{-1}), and μ is Poisson's ratio. These parameters allow for the determination of the critical value of the temperature function T_{rr} and the corresponding onset of tensile stresses σ^+. Similarly, when using the compressive strength limit σ^-, the critical value of the temperature function $T_{\phi\phi}$, which is responsible for compressive stresses, is defined. These stresses allow for a quantitative assessment of the probability of failure in the surface layers of small bodies. Below, Table 1 presents the thermal and elastic properties of crystalline ice at low temperatures.

In work Klinger (1981), the thermal conductivity of crystalline ice for temperatures above 25 K was defined as a temperature function, while the heat capacity was determined from experimental data in the temperature range of 16.43 $K \leqslant T \leqslant 267.77$ K and is approximated by the expression provided in work Klinger (1980). Consequently, the thermal diffusivity of crystalline ice can be obtained using the formula $a^2 = \frac{\kappa}{c_v}$ and the final expression is written as a temperature function:

$$a^2 = \frac{5.67}{0.92T(7.49 * 10^{-3}T + 0.09)} \text{ cm}^2\text{sec}^{-1}, \quad (1)$$

Subsequently, Table 2 presents the adopted values of the material parameters and their corresponding temperature functions for minerals, rocks, basalt, and chondrites Shestakova et al. (2019).

In our research, the data for thermal conductivity and heat capacity were sourced from the findings in Opeil et al. (2012), where thermal conductivity was measured for seventeen stony meteorites across a temperature range from 5 K to 300 K. The

Table 1. Material parameters for ice in SI units

	c_v	κ	a^2	α	μ	E	T_-	σ_-	T_+	σ_+
T (K)	erg/cm^3 K	erg/(s cm K)	cm^2/s	1/K	–	MPa	K	MPa	K	MPa
30	0.3147×10^7	1.89×10^6	0.6	–	–	–	–	–	–	–
125	1.026×10^7	0.4536×10^6	0.0442	3.8×10^{-5}	0.33	9×10^3	-10	-5	4	2

Table 2. Physico-mechanical parameters of stone meteorites

Parameter	a^2 cm^2/s	α 1/K	μ –	E MPa	T_- K	σ_- MPa	T_+ K	σ_+ MPa
Minerals	0.0058	7.5×10^{-6}	0.15	72000	-1300	-800	130	80
Rocks				26000	-800	-180	90	20
Basalt	0.0167		0.25	7×10^4	-300	-160	7	4.5
Carbon chondrites	0.0118				-86	-60	13	9
Ordinary chondrites					-214	-150	36	25

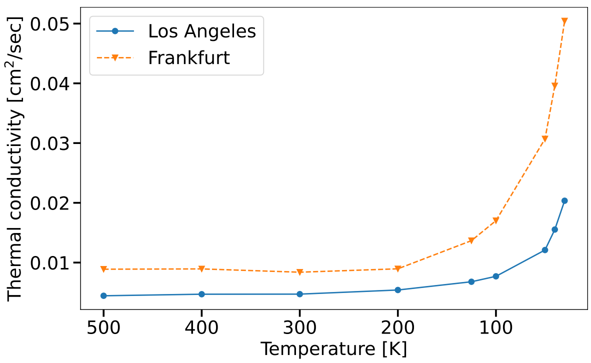

Figure 1. Thermal diffusivity a^2 for meteorite samples

selection of this specific rock type is based on the fact that, for instance, the Frankfurt meteorite (a howardite) serves as a typical sample of the material found on the surface of the asteroid Vesta. The thermal conductivity of these meteorites, as measured by Opeil Opeil et al. (2012), is described by a fourth-order equation of the following form:

$$K = A + BT + CT^2 + DT^3 + ET^4 \tag{2}$$

The coefficients for the Frankfurt basaltic chondrite sample at temperatures of 300 K and below were utilized Opeil et al. (2012). The selected parameters are listed in Table 3.

For numerical simulations, data from the bottom row of Table 3 for the Los Angeles sample is used, while analytical calculations are based on Table 3. The temperature dependencies are illustrated in Fig. 1.

Approximating a^2 (Los Angeles) by a polynomial, we obtain:

$$a^2(T) = (3.7404 \cdot 10^{-12}T^4 - 4.6002 \cdot 10^{-9}T^3 + 1.9825 \cdot 10^{-6}T^2 - 3.5451 \cdot 10^{-4}T + 2.7446 \cdot 10^{-2})\ \mathrm{cm^2 s^{-1}} \tag{3}$$

3 NUMERICAL SOLUTION OF THE THERMAL DIFFUSION EQUATION AND CALCULATION OF THERMAL STRESSES FOR SMALL BODIES

The boundary value problem for the thermal diffusion equation (HDE) for a spherical body according to Shestakova & Tambovtseva (1997) is written as:

$$\frac{\partial T}{\partial t} = a^2 \frac{\partial^2 T}{\partial x^2} + \frac{2a^2}{x}\frac{\partial T}{\partial x} \tag{4}$$

$$T(r, 0) = T_0, \tag{5}$$

$$\frac{dT(0,t)}{dx} = 0, \tag{6}$$

$$T_d(r,t) = \frac{T_0}{(1 - \frac{t}{\tau_0})^{\frac{1}{3}}} \tag{7}$$

Equation 4 defines the initial condition for the surface temperature at the initial moment of time. Expressions 6 and 7 represent the boundary conditions, where the former accounts for the spherical symmetry of the heat flux, and the latter 5 defines the surface temperature of the small body in the blackbody approximation: $T_0 = T_* \sqrt{\frac{R_*}{2R}}$. Equation 4 is solved numerically, where $T(x,t)$ is the temperature, and the thermal diffusivity $a^2(T)$, is determined by empirical formulas depending on temperature for crystalline ice Eq. 1 and silicate rock Eq. 3. The numerical scheme employed is the explicit Euler method. After obtaining the temperature profile $T(x,t) \to T(y)$ from the surface to the center of the spherical body, $T(y)$ is substituted into the expressions for thermal stresses.

$$T_{\phi\phi}(x) = \frac{2}{r^3}\int_0^r T(y)y^2dy + \frac{1}{x^3}\int_0^x T(y)y^2dy - T(x), \tag{8}$$

Table 3. Thermal parameters of meteorite samples Frankfurt and Los Angeles

Temperature (K)	**500**	**400**	**300**	**200**	**125**	**100**	**50**	**40**	**30**
k (W/m) Frankfurt	2	1,9	1,6356	1,2876	1,2648	1,2336	0,9214	0,7916	0,6305
k (W/m) Los Angeles	1,1	1	0,9204	0,7774	0,6284	0,5584	0,36209	0,310748	0,254429
c_p (J/(kg K))	900	850	780	575	370	290	120	80	50
a^2 Los Angeles	0,00444	0,004706	0,00472	0,00541	0,0067	0,00770	0,0121	0,0155	0,0203
a^2 Frankfurt	0,0088	0,0089	0,0083	0,0089	0,013	0,017	0,030	0,0395	0,0504

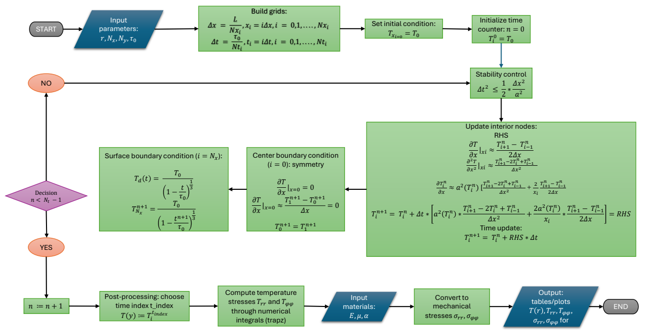

Figure 2. Block diagram of the numerical solution of the HDE and calculation of thermal stresses

$$T_{rr}(x) = \frac{2}{r^3}\int_0^r T(y)y^2dy - \frac{2}{x^3}\int_0^x T(y)y^2dy, \tag{9}$$

By using temperature functions as analogues of thermal stresses, we can readily convert them to the actual stresses using the following simple relationship:

$$\sigma_{\phi\phi}(x) = \frac{E\alpha}{1-\mu}T_{\phi\phi}(x), \quad \sigma_{rr}(x) = \frac{E\alpha}{1-\mu}T_{rr}(x), \tag{10}$$

The notations are provided in Section 2, and the results for the temperature profiles and stresses will be presented in Section 3. Below is the numerical algorithm for solving Equation 4 using the explicit Euler scheme with the initial condition Eq. 5 and two boundary conditions Equations 6 and 7, followed by the calculation of stresses using formulas 8, 9 and 10 Tambovtseva & Shestakova (1999); Boley & Weiner (1960).

The analytical calculation of HDE and thermal stresses is presented in Shestakova & Tambovtseva (1997). Further in the next section, comparisons of analytical and numerical approaches will be presented.

4 COMPARISON OF ANALYTICAL AND NUMERICAL METHODS FOR SMALL BODIES. DISCUSSION.

Analytical method: This method is based on a simplified model where thermal conductivity and diffusivity are assumed to be temperature-independent. It allows for the rapid acquisition of temperature functions and thermal stresses. The model accurately describes the behavior of temperature and stress near the surface and in the center of the bodies. The primary limitation is inaccuracy in the intermediate layers, particularly for large bodies (radius > 1 km).

Numerical method: This method solves the nonlinear heat conduction equation with temperature-dependent thermal diffusivity $a^2(T)$. This approach is suitable for large bodies as well. Below, the simulation results of both approaches for bodies composed of crystalline ice and silicates are presented.

Crystal Ice: For the numerical calculation of crystalline ice, the variable coefficient from Eq. 1 was used, while for the analytical solution, a constant a^2 was adopted according to Table 1. For small cometary bodies, the value of a^2 was taken at $T = 30$ K; for large bodies, the value was taken at $T = 125$ K; and for medium-sized bodies, a^2 was averaged over the temperature range $T = (30-125)$ K. The calculated temperature and stress profiles are presented below in Figure 3.

As shown in Figure 3, when the radius of the ice bodies reaches 1 km or 3.5 km, the results of the analytical and numerical methods practically coincide. However, as the body size decreases for instance, to 200 m and 30 m a certain divergence in the results is observed, although the error remains relatively small. Figure 3 presents a comparison of the numerical and analytical solutions for bodies of various sizes. For all bodies, a high degree of agreement is observed in the near-surface zone. For a cometary body with a radius of 30 m, the average discrepancy between the analytical and numerical methods is 1.56 K, which corresponds to a 5% relative error; the maximum discrepancy is 4 K near the center. Discrepancies are minimal (less than 1 K) at a 10% relative depth x/r. For a 200 m cometary body, the average discrepancy is 2.1 K, with a maximum of approximately 5 K near the center. For a 1 km body, the average discrepancy is approximately 1.09 K, with a maximum of about 2.5 K near the center. For a 3.5 km body, the discrepancy is negligible, remaining less than 1 K across the entire profile. For small bodies (less than 30 m), discrepancies arise at depth due to the finite size of the body and effects associated with rapid heating.

Subsequently, Figure 4 illustrates the dependence of radial stresses at the center and tangential stresses at the surface as a function of distance, obtained by both analytical and numerical methods.

The solutions obtained for small bodies demonstrate good agreement between the numerical and analytical approaches, as only minor discrepancies in stresses are observed at different distances, as shown in Figure 4. For a cometary body with a radius of 30 m, the discrepancies in radial stresses at the center are less than 0.5 K from the starting position to the final distance; however, at the final distance, a difference of approximately 5 K is observed. This result is consis-

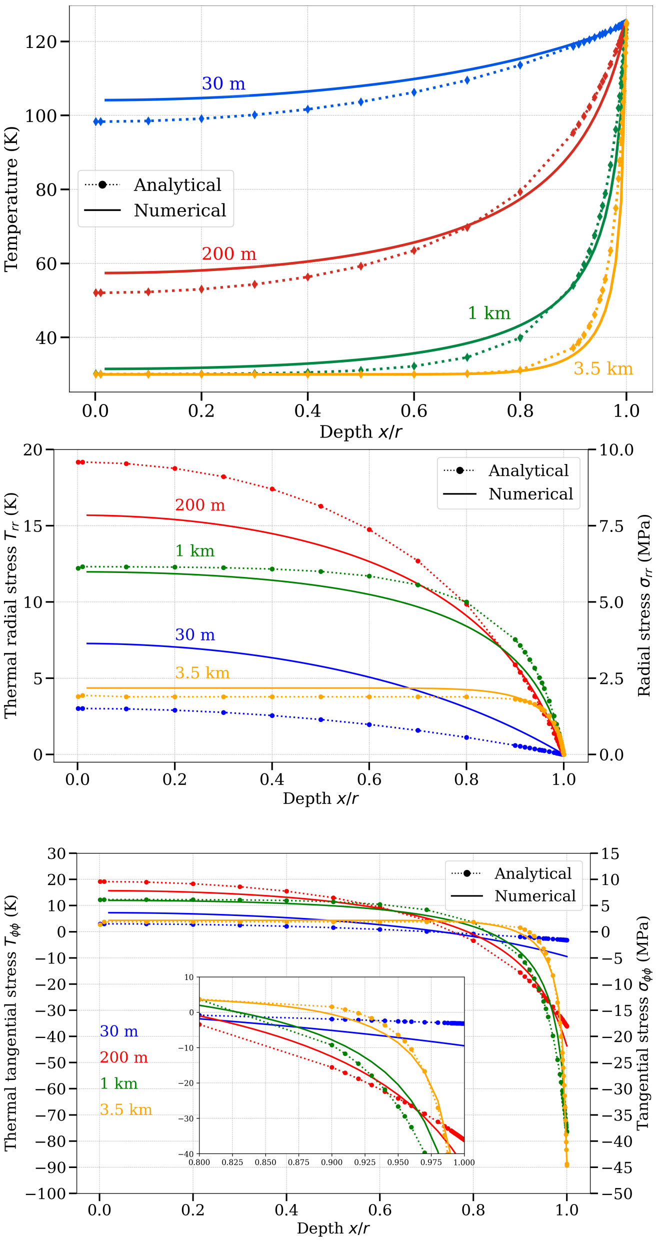

Figure 3. Profiles of temperature, as well as radial and tangential thermal stresses, from the surface to the center of the crystal ice small bodies at a final distance of 4.95 AU, obtained by both analytical (a^2 = const) and numerical methods.

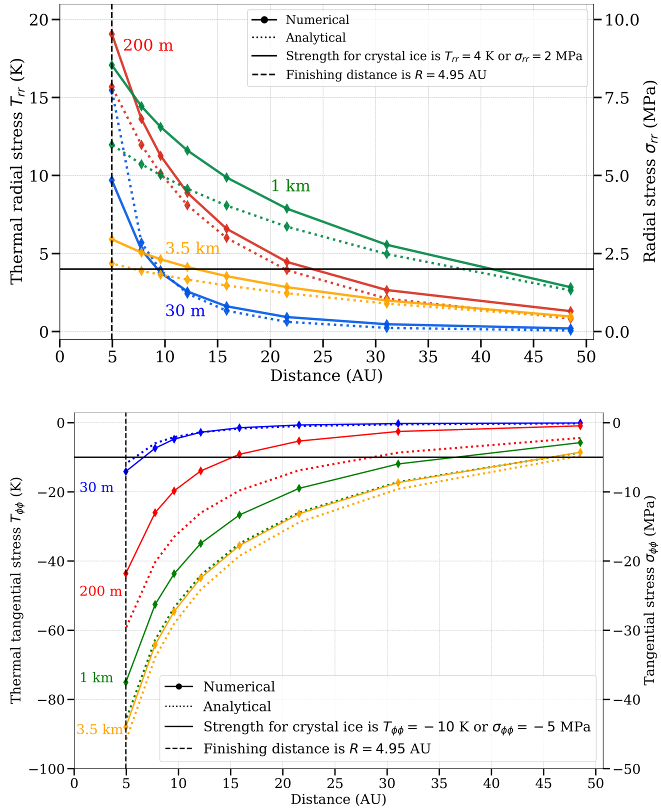

Figure 4. Thermal stresses at the center of the body (x/r=0) for the radial component (left) and at the surface (x/r=1) for the tangential component (right), calculated by analytical and numerical methods at various heliocentric distances from the initial position of 86 AU to the final distance of 4.95 AU.

tent with the stress discrepancies shown in Figure 3. For a cometary body with a radius of 200 m, the average discrepancy in stresses at the center is about 1 K from the start to the final distance, while at the final distance the discrepancy reaches approximately 4 K. For a cometary body with a radius of 1 km, stress discrepancies are observed at almost all distances, with an average discrepancy of about 5 K and a maximum discrepancy at the final distance of approximately 10 K. For a cometary body with a radius of 3.5 km, the average discrepancy is about 1.5 K, with a maximum discrepancy at the final distance of approximately 2 K. Such minimal discrepancies can be explained by the fact that, in the analytical solution (HDE), a constant value of the a^2 parameter is used at T = 30 K for bodies larger than 1 km, since they retain an initially low temperature in their central regions up to the moment of destruction. For bodies with radii of approximately 30 m, a^2 - constant value is used at T = (125–200) K, corresponding to the blackbody temperature at the final distance, as heating in such bodies occurs throughout the entire volume. However, for sub-kilometer bodies, this parameter is averaged over the temperature range between the start and final distances, T = (30 – 200) K, since pronounced temperature gradients are observed throughout the entire profile. Further, Figure 5 show the temperature profile, thermal radial and tangential stresses in the near-surface layer at a depth of 10 m.

As shown in Figure 5, heating occurs more effectively for the cometary body with a radius of 30 m, while the results for radii of 200 m, 1 km, and 3.5 km are comparable. The temperature discrepancy at a depth of 10 m between the two methods is approximately 10 K. The temperature discrepancy at a depth of 10 m between the two methods is approximately 10 K. For the stresses shown in Figure 5, the discrepancy between the analytical and numerical methods at a depth of 10 m is about 1 K for the 30 m and 200 m bodies, whereas for the 1 km and 3.5 km bodies the discrepancy is minimal (less than 0.1 K). For the stresses in Figure 5,

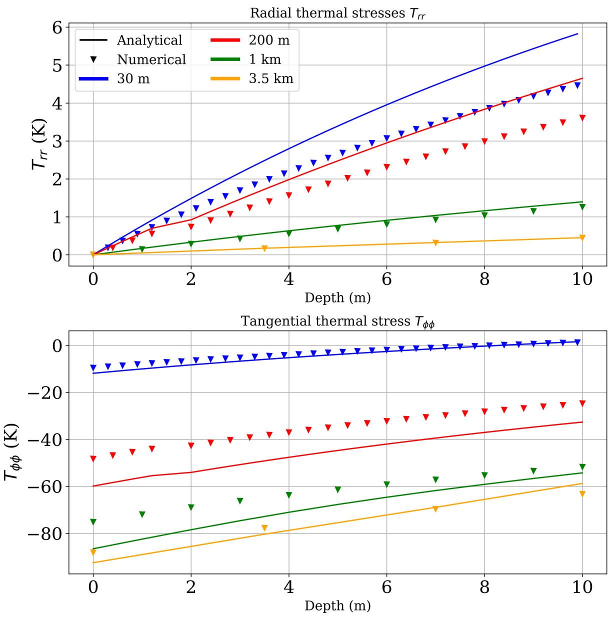

Figure 5. Profiles of radial and tangential thermal stresses in the near-surface layer at a depth of 10 m at a final distance of 4.95 AU, obtained by analytical (solid curve) and numerical (dotted curve) methods for cometary bodies of various sizes.

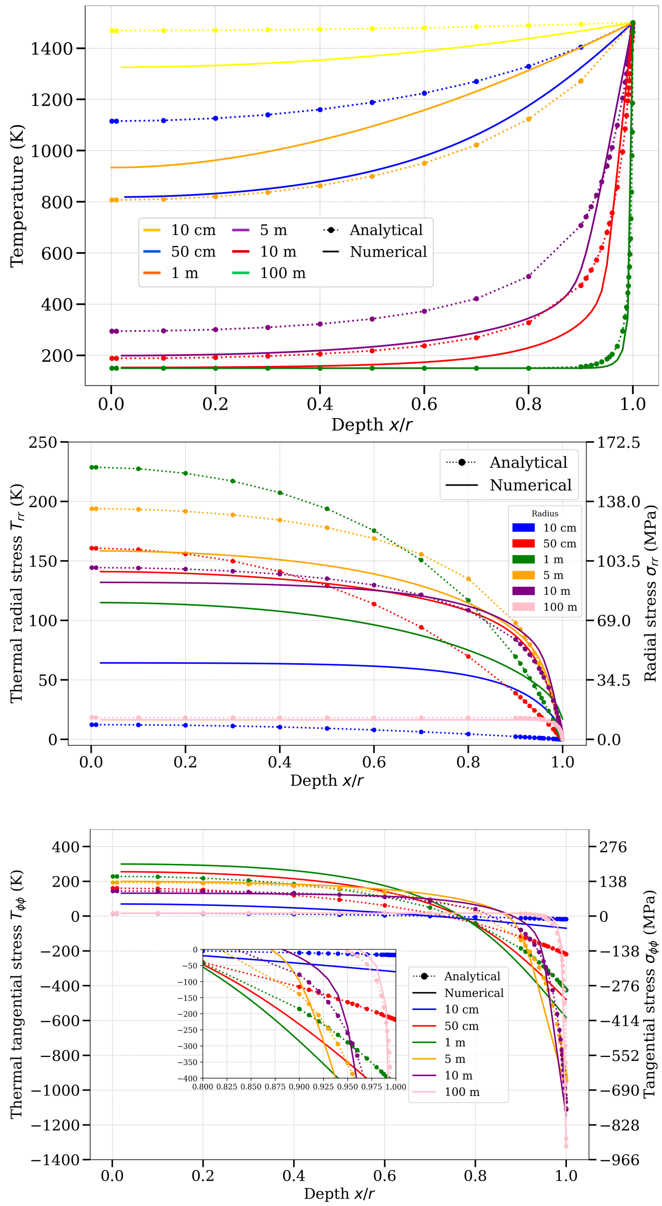

Figure 6. Profiles of temperature, as well as radial and tangential thermal stresses, from the center (x/r=0) to the surface (x/r=1) within bodies of various sizes at a final heliocentric distance of 0.0345 AU $\approx 7.4\, R_\odot$ for chondritic material, obtained by both analytical (a^2 = const) and numerical methods.

the discrepancy for the 30 m body is less than 1 K, while for the 200 m, 1 km, and 3.5 km bodies it is approximately 10 K. It is also important to note with regard to Figure 5, which is also applicable to silicate rocks, that at the surface $|x = r|$ the radial stress is $T_{rr} = 0$, whereas the tangential stress is $T_{\varphi\varphi} < 0$. However, as depth increases toward the center, the stresses T_{rr} and $T_{\varphi\varphi}$ should begin to equalize, a behavior that should be consistent for both methods. An analysis of crystalline ice clearly demonstrates this trend for a cometary body with a radius of 30 m, since a depth of 10 m constitutes one-third of its profile. A comparison of the results shows that at a depth of 10 m $T_{rr} \approx T_{\varphi\varphi}$, with values of approximately 5 K for the analytical method and 6 K for the numerical method. For cometary bodies with radii of 200 m, 1 km, and 3.5 km, such equalization is not observed, because a depth of 10 m represents only a small fraction of the total profile. The analytical solution performs well for large bodies, for which thermal diffusion does not reach the center and the temperature distribution remains relatively stable. However, for small bodies, where the entire volume heats up rapidly, only the numerical model accurately reflects the temporal and spatial variations in temperature.

Silicates: For the numerical calculations of silicate rocks, the variable coefficient from Equation 3 was used, whereas a constant value was adopted for basalt and chondrites in the analytical solution in accordance with Table 2. Figure 6 illustrates the temperature profiles, as well as the radial and tangential thermal stresses, within meteoroid bodies.

Figure 6 presents a comparison of the numerical and analytical solutions of the heat diffusion equation for small bodies with radii of 10 cm, 50 cm, 1 m, 5 m, 10 m, and 100 m composed of silicate chondritic and basaltic material. For a 100 m meteoroid, a nearly complete coincidence of the numerical and analytical temperature and stress profiles is observed, with differences of less than 1 K. For radii of 1 m and 5 m, the average discrepancy is approximately 20 K. For bodies of 10 cm and 50 cm, the average discrepancy is about 200 K, which is considered a reasonable result given that the blackbody temperature at the final distance is 1500 K. The highest level of agreement (with discrepancies of less than 20 K) occurs in the near-surface region, extending up to 5% of the total profile. However, the maximum discrepancies occur at the center: 150 K for 10 cm, 300 K for 50 cm, 100 K for 1 m, 100 K for 5 m, 50 K for 10 m, and 5 K for 100 m. Significant

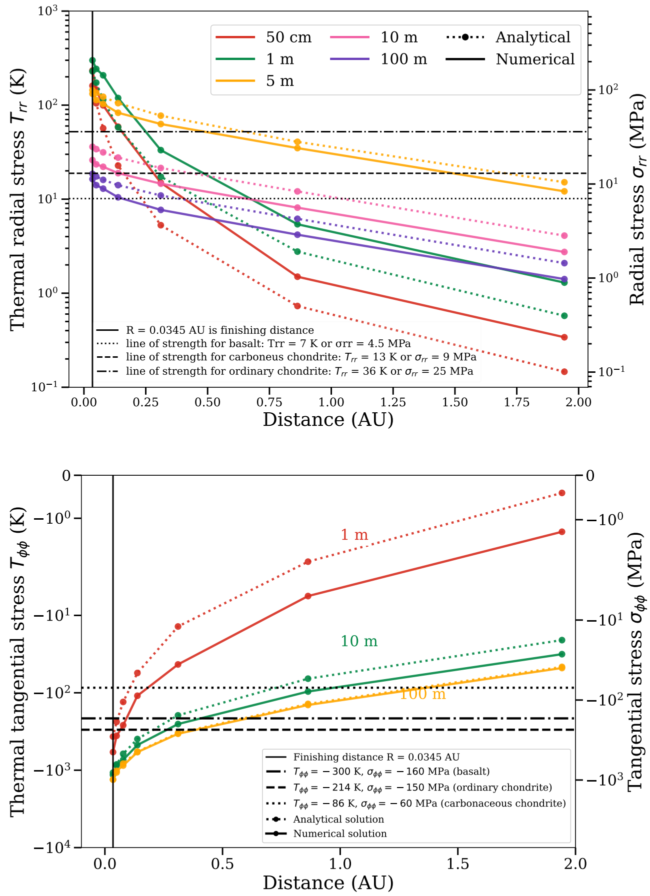

Figure 7. Thermal stresses at the center of the body (x/r=0, radial component) and at the surface (x/r=1, tangential component), calculated using analytical and numerical methods at various heliocentric distances from the initial position of 3.45 AU to the final distance of 0.0345 AU $\approx 7.4\,R_{\odot}$ for chondritic and basaltic bodies.

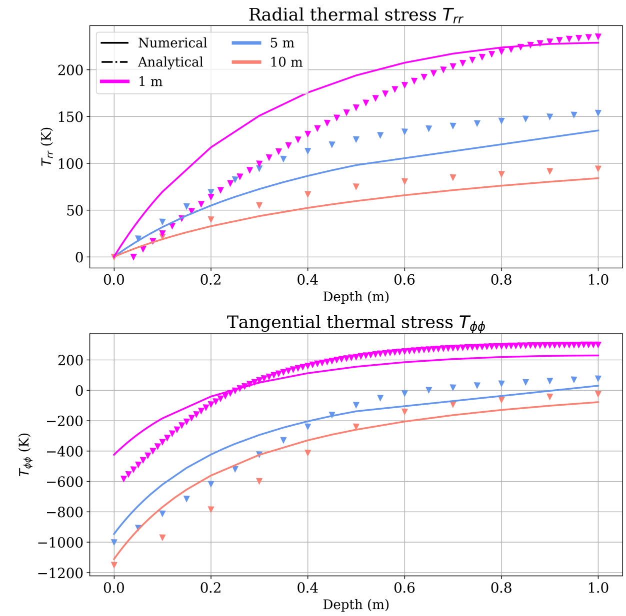

Figure 8. Profiles of radial and tangential thermal stresses in the near-surface layer at a depth of 1 m at a final heliocentric distance of 0.0345 AU $\approx 7.4\,R_{\odot}$, obtained by analytical (solid curve) and numerical (dotted curve) methods for meteoroids of chondritic and basaltic material of various sizes.

discrepancies are observed throughout the entire volume for bodies with radii of 10 cm and 50 cm. Due to their small size, heating encompasses nearly the entire volume, and the temperature gradient equalizes rapidly. Thus, as with icy bodies, the analytical solution for silicate meteoroids proves accurate only when there is a sufficient thickness of the uncooled layer, whereas the numerical model is necessary for an adequate description of thermal processes in small bodies.

Subsequently, Figure 7 illustrates the dependence of radial stresses at the center and tangential stresses at the surface on the distance from the star, obtained by both analytical and numerical methods. These dependencies are calculated specifically for silicate bodies.

Analysis of Figure 7 shows that for bodies with radii from 1 m to 100 m, both stress calculation approaches at different distances demonstrate good agreement, and discrepancies in distances are minimal. For a body with a radius of 50 cm, the average discrepancy is approximately 100 K; for 1 m, it is 80 K; for 5 m, 20 K; for 10 m, 50 K; and for 100 m, 45 K. The stresses at the final distance also differ for all sizes. The discrepancy between the two methods varies: for 50 cm, it is about 50 K; for 1 m, 100 K; for 1 m and 5 m, approximately 100 K; for 10 m, 50 K; and for 100 m, about 10 K. Subsequently, Figure 8 presents the profiles of temperature, as well as radial and tangential thermal stresses, in the near-surface layer at a depth of 1 m for small silicate bodies. An analysis of the near-surface layer presented in Figure 8 was carried out in a manner similar to that described for Figure 5. The main difference lies in the fact that the near-surface layer was considered at a depth of 1 m, which is associated with the lower thermal conductivity of silicates compared to crystalline ice. As shown in Figure 8, the temperature discrepancies between the analytical and numerical methods are small: approximately 5 K for a meteoroid with a radius of 1 m, 15 K for a radius of 5 m, and 10 K for a radius of 10 m. Regarding the stresses in Figure 8, the discrepancy is about 50 K for the 1 m body, approximately 10 K for the 5 m body, and about 30 K for the 10 m body. Furthermore, the equalization condition $T_{rr} \approx T_{\varphi\varphi}$ occurs at a depth of 40 cm for a 1 m radius meteoroid at a temperature of approximately 150 K according to the numerical method, and at a depth of 50 cm at the same temperature for the analytical method. For the 5 m and 10 m bodies, this equalization is expected to occur at depths greater than 1 m from the surface. The numerical model is applicable to silicate bodies and shows consistency with the analytical solution. For large silicate bodies with radii exceeding 10 m, the temperature distribution remains stable in both the deep interior and near-surface layers, since thermal diffusion does not reach the center due to the low thermal conductivity of silicates, whose thermal diffusivity is approximately an order of magnitude smaller than that of crystalline ice. For this reason, a narrower size range from 10 cm to 100 m was selected, as even a 10 m fragment retains its initial temperature in the central region. For small silicate bodies (less than 1 m), where the entire volume heats rapidly, only the numerical model accurately describes the temporal and spatial evolution of temperature. The proposed numerical model is applicable to both silicate and icy bodies. Similarities and discrepancies follow the same general trends for both large and small bodies; the primary difference lies in the selected size range: from 10 cm to 100 m for silicates and from 30 m to 3.5 km for icy bodies.

To address the physical interpretation of the comparison,it should be noted that the observed minor discrepancies between the two approaches are primarily driven by the temperature dependence of the thermal diffusivity a^2(T), rather than numerical artifacts. In the numerical approach, the nonlinear heat conduction equation is solved using the explicit Euler finite-difference scheme (first-order in time and second-order in space, FTCS) to account for the dynamically changing a^2(T), and the resulting temperature field is subsequently used to calculate thermal stresses. Despite the differences in the mathematical treatment, the analytical method demonstrates very good overall agreement. This is due to the careful selection of the constant a^2 based on the physical characteristics of the bodies. Specifically, for very large bodies, a^2 was chosen at the initial temperature, since their internal regions remain cold until the final distance. For small bodies, which heat up entirely, a^2 was taken at the temperature corresponding to the final distance. For medium-sized bodies, an averaged a^2 between the initial and final temperatures was used. Because of this size-dependent parametrization, the analytical model successfully minimizes deviations from the numerical solution, resulting in only slight differences in the evaluated thermal gradients and stresses.

5 CONCLUSIONS

This study formulates and solves a comprehensive problem addressing the mechanism of thermal destruction of small bodies (SB) of various compositions (icy and silicate) during their approach to the Sun.

Key Results

The following dependencies of destruction on the size and composition of stony bodies have been established:

- Basaltic and carbonaceous bodies begin to disintegrate at heliocentric distances between Earth's orbit and Mars's orbit (1–2.5 AU).
- Ordinary chondrites disintegrate closer to Venus's orbit (∼0.7 AU).
- Small stony bodies (< 10 m) disintegrate in the region between the orbits of Mars and Mercury, while larger bodies (∼40–100 m) disintegrate between the orbits of Mercury and Venus.
- Very large silicate bodies (> 100 m) disintegrate closer to the Sun, producing dust clouds observable in the infrared and optical ranges.

For cometary nuclei moving along highly eccentric orbits, thermal stresses generated by the heating of surface layers are shown to be a critical factor in their destruction. Bodies with radii from 100 m to 3 km are most susceptible to internal cracking due to strong temperature gradients between the cold interior and the heated surface. Small bodies (radius up to 10 m) heat throughout their entire volume without accumulating significant internal stresses, whereas large bodies (radius greater than 10 km) retain a cold interior and experience heating only in a thin surface layer, remaining resistant to thermal destruction.

- For small bodies composed of silicates (0.1–5 m) and crystalline ice (less than 30 m), the analytical solution may significantly deviate in the central regions, whereas the numerical solution accurately accounts for volumetric heating.
- For icy bodies (30–200 m) and silicate bodies (10–100 m), the analytical solution remains applicable in the near-surface zone (up to 10–20% of the radius), but numerical modeling is required at greater depths.
- For large bodies (1–3.5 km for cometary nuclei and ∼100 m for silicates), discrepancies between the analytical and numerical approaches are minimal throughout the entire profile.

Both approaches complement each other effectively, and their combined application provides a reliable and accurate assessment of the stability of small bodies during solar approach.

In the long term, this research may be extended by incorporating elliptical orbits and modeling multiple orbital revolutions up to the complete destruction and subsequent evaporation of cometary nuclei. This would allow for consideration of thermal stresses arising both during the approach to and recession from the star. Future developments include more detailed calculations of mass loss during stellar approaches and subsequent material accretion. Additional modeling will account for various heat balance boundary conditions, internal sublimation processes, and other relevant physical factors. Further refinement may be achieved by integrating multiple destruction mechanisms and orbital dynamics into a comprehensive simulation framework describing the environment of both the star and the small body. The model is planned to be extended to three dimensions with implementation of the full thermal stress tensor. Moreover, diurnal rotation effects will be incorporated, including azimuthal and latitudinal (equatorial) profiles and their influence on thermal stress distribution.

FUNDING

The work is carried out within the framework of: the Project No. BR24992807 «Development of Kazakhstan digital environment for astronomical research of near and deep space objects within the international virtual observatory network» and Project No. BR24992759 «Development of the concept for the first Kazakhstani orbital cislunar telescope – Phase

I», financed by the Ministry of Science and Higher Education of the Republic of Kazakhstan)

REFERENCES

Sekanina Z., Chodas P. W., Yeomans D. K., 1994, A&A, **289**, 607–613
Solem J. C., 1995, A&A, **302**, 596–600
Jewitt D., 2022, AJ, **164**, 158
Sekanina Z., 1997, A&A, **318**, L5–L8
Boehnhardt H., 2005, in *Comets II*, **1**, 301–316
Brož M., et al., 2024, A&A, **689**, A183
Jewitt D., 2010, AJ, **140**, 1519–1527
Shestakova L. I., Serebryanskiy A. V., 2023, MNRAS, **524**, 4506–4520
Shestakova L. I., Tambovtseva L. V., 1997, Earth Moon Planets, **76**, 19–45
Shestakova L. I., Spassyuk R., Omarov C., 2025, MNRAS, **in press**, doi:10.1093/mnras/staf081
Prialnik D., Jewitt D., 2022, arXiv e-prints, **2209.05907**
Grundy W. M., et al., 2006, Icarus, **184**, 543–555
Guilbert A., et al., 2009, Icarus, **201**, 272–283
de Bergh C., et al., 2009, Icarus, **201**, 272–283
Brown R. H., Calvin W. M., 2000, Science, **287**, 107–109
MacLennan E. M., Granvik M., 2023, LPI Contrib., **2851**, 2431
MacLennan E., Granvik M., 2024, Nat. Astron., **8**, 60–68
Tambovtseva L. V., Shestakova L. I., 1999, Planet. Space Sci., **47**, 319–326
Täuber F., Kührt E., 1987, Icarus, **69**, 83–90
Čapek D., Vokrouhlický D., 2010, A&A, **519**, A75
Klinger J., 1981, Icarus, **47**, 320–324
Klinger J., 1980, Science, **209**, 271–272
Shestakova L. I., Demchenko B. I., Serebryanskiy A. V., 2019, MNRAS, **487**, 3935–3945
Opeil C. P., et al., 2012, Meteorit. Planet. Sci., **47**, 319–329
Boley B. A., Weiner J. H., 1960, *Theory of Thermal Stress*, **1**, 302